Mon. Not. R. Astron. Soc. **396,** 2419–2432 (2009) doi:10.1111/j.1365-2966.2009.14920.x

The first outburst of the new magnetar candidate SGR 0501+4516

N. Rea,[1⋆] G. L. Israel,[2] R. Turolla,[3,4] P. Esposito,[5,6] S. Mereghetti,[5] D. Götz,[7] S. Zane,[4] A. Tiengo,[5] K. Hurley,[8] M. Feroci,[9] M. Still,[4] V. Yershov,[4] C. Winkler,[10] R. Perna,[11] F. Bernardini,[2] P. Ubertini,[9] L. Stella,[2] S. Campana,[12] M. van der Klis[1] and P. Woods[13]

[1]*Astronomical Institute 'Anton Pannekoek', University of Amsterdam, Science Park 904, Postbus 94249, 1090 GE, Amsterdam, the Netherlands*
[2]*INAF – Osservatorio Astronomico di Roma, via Frascati 33, 00040 Monte Porzio Catone (RM), Italy*
[3]*Università di Padova, Dipartimento di Fisica, via Marzolo 8, I-35131 Padova, Italy*
[4]*Mullard Space Science Laboratory, University College London, Holmbury St Mary, Dorking, Surrey RH5 6NT*
[5]*INAF – Istituto di Astrofisica Spaziale e Fisica Cosmica, via E. Bassini 15, I-20133 Milano, Italy*
[6]*INFN – Istituto Nazionale di Fisica Nucleare, Sezione di Pavia, via A. Bassi 6, 27100 Pavia, Italy*
[7]*CEA Saclay, DSM/Irfu/Service d'Astrophysique, Orme des Merisiers, Bât. 709, 91191 Gif sur Yvette, France*
[8]*University of California, Space Sciences Laboratory, 7 Gauss Way, 94720-7450 Berkeley, USA*
[9]*INAF – Istituto di Astrofisica Spaziale e Fisica Cosmica, via Fosso del Cavaliere 100, I-00133 Rome, Italy*
[10]*Astrophysics Division, Research and Scientific Support Department, ESA-ESTEC, Keplerlaan 1, 2201 AZ Noordwijk, the Netherlands*
[11]*JILA, University of Colorado, Boulder, CO 80309-0440, USA*
[12]*INAF – Osservatorio Astronomico di Brera, Via Bianchi 46, I-23807 Merate (Lc), Italy*
[13]*Dynetics, Inc., 1000 Explorer Boulevard, Huntsville, AL 35806, USA*

Accepted 2009 April 15. Received 2009 April 9; in original form 2009 March 9

ABSTRACT

We report here on the outburst onset and evolution of the new soft gamma-ray repeater SGR 0501+4516. We monitored the new SGR with *XMM–Newton* starting on 2008 August 23, 1 day after the source became burst active, and continuing with four more observations in the following month, with the last one on 2008 September 30. Combining the data with the *Swift* X-ray telescope (*Swift*–XRT) and *Suzaku* data, we modelled the outburst decay over a 3-month period, and we found that the source flux decreased exponentially with a time-scale of $t_c = 23.8$ d. In the first *XMM–Newton* observation, a large number of short X-ray bursts were observed, the rate of which decayed drastically in the following observations. We found large changes in the spectral and timing behaviour of the source during the first month of the outburst decay, with softening emission as the flux decayed, and the non-thermal soft X-ray spectral component fading faster than the thermal one. Almost simultaneously to our second and fourth *XMM–Newton* observations (on 2008 August 29 and September 2), we observed the source in the hard X-ray range with *INTEGRAL*, which clearly detected the source up to ∼100 keV in the first pointing, while giving only upper limits during the second pointing, discovering a variable hard X-ray component fading in less than 10 days after the bursting activation. We performed a phase-coherent X-ray timing analysis over about 160 days starting with the burst activation and found evidence of a strong second derivative period component [$\ddot{P} = -1.6(4) \times 10^{-19}$ s s^{-2}]. Thanks to the phase connection, we were able to study the phase-resolved spectral evolution of SGR 0501+4516 in great detail. We also report on the *ROSAT* quiescent source data, taken back in 1992 when the source exhibits a flux ∼80 times lower than that measured during the outburst, and a rather soft, thermal spectrum.

Key words: pulsars: general – pulsars: individual: SGR 0501+4516.

1 INTRODUCTION

Over the last few years, a number of observational discoveries have placed 'magnetars' (ultramagnetized isolated neutron stars) in the limelight again. These extreme objects comprise the anomalous X-ray pulsars (AXPs; 10 objects), and the soft gamma-ray

⋆E-mail: n.rea@uva.nl

repeaters (SGRs; four objects), which are observationally very similar classes in many respects (for a recent review, see Mereghetti 2008). They are all slow X-ray pulsars with spin periods clustered in a narrow range ($P \sim 2$–12 s), relatively large period derivatives ($\dot{P} \sim 10^{-13}$ to 10^{-10} s s^{-1}), spin-down ages of 10^3–10^4 years and magnetic fields, as inferred from the classical magnetic dipole spin-down formula, of 10^{14}–10^{15} G, much higher than the electron quantum critical field ($B_{\rm cr} \simeq 4.4 \times 10^{13}$ G). About a dozen AXPs and SGRs are strong persistent X-ray emitters, with X-ray luminosities of about 10^{34}–10^{36} erg s^{-1}, and a few transient ones have been discovered in recent years. A peculiarity of these neutron stars is that their X-ray energy output is much larger than their rotational energy losses, so they cannot be only rotationally powered. Furthermore, they lack a companion, so they cannot be accretion powered either. Rather, the powering mechanism of AXPs and SGRs is believed to reside in the neutron star ultrastrong magnetic field (Duncan & Thompson 1992; Thompson & Duncan 1993). Other scenarios, beside the 'magnetar' model, were proposed to explain AXP and SGR emission, such as the fossil disc (Chatterjee, Hernquist & Narayan 2000; Perna, Hernquist & Narayan 2000) and the quark-star model (Ouyed, Leahy & Niebergal 2007a,b).

In the 0.1–10 keV energy band, magnetars spectra are relatively soft and empirically modelled by an absorbed blackbody (BB; $kT \sim 0.2$–0.6 keV) plus a power law (PL; $\Gamma \sim 2$–4). Thanks to *INTEGRAL*–ISGRI and *RXTE*–HEXTE, hard X-ray emission up to $\sim$200 keV has recently been detected from some sources (Kuiper, Hermsen & Mendez 2004; Kuiper et al. 2006; Mereghetti et al. 2005; Götz et al. 2006). This discovery has opened a new window on magnetars studies and has shown that their energy output may be dominated by hard, rather than soft emission.

At variance with other isolated neutron stars, AXPs and SGRs exhibit spectacular episodes of bursting and flaring activity, during which their luminosity may change up to 10 orders of magnitude on time-scales down to few milliseconds. Different types of X-ray flux variability have been observed, ranging from slow and moderate flux changes up to a factor of a few on time-scales of years (shown by virtually all members of the class) to more intense outbursts with flux variations up to $\sim$100 lasting for $\sim$1–3 years and to short and intense X-ray burst activity on subsecond time-scales (see Kaspi 2007 and Mereghetti 2008 for reviews of X-ray variability).

In particular, SGRs are characterized by periods of activity during which they emit numerous *short bursts* in the hard X-ray/soft gamma-ray energy range ($t \sim 0.1$–0.2 s; $L \sim 10^{38}$–10^{41} erg s^{-1}). This is indeed the defining property that led to the discovery of this class of sources. In addition, they have been observed to emit *intermediate flares*, with typical durations of $t \sim 1$–60 s and luminosities of $L \sim 10^{41} - 10^{43}$ erg s^{-1}, and spectacular *giant flares*. The latter are rare and unique events in the X-ray sky, by far the most energetic ($\sim 10^{44}$–10^{47} erg s^{-1}) Galactic events currently known, second only to Supernova explosions. Indeed, the idea that SGRs host an ultramagnetized neutron star was originally proposed to explain the very extreme properties of their bursts and flares: in this model, the frequent short bursts are associated with small cracks in the neutron star crust, driven by magnetic diffusion, or, alternatively, with the sudden loss of magnetic equilibrium through the development of a tearing instability, while the giant flares would be linked to global rearrangements of the magnetic field in the neutron stars magnetosphere and interior (Thompson & Duncan 1995; Lyutikov 2003).

Bursts and flares do not seem to repeat with any regular, predictable pattern. Giant flares have been so far observed only three times from the whole sample of SGRs [from SGR 0526−66 in 1979 (Mazets et al. 1979), from SGR 1806−20 in 1998 (Hurley et al. 1999) and from SGR 1900+14 in 2004 (e.g. Hurley et al. 2005; Palmer et al. 2005)], and never twice from the same source. As far as short bursts and intermediate flares are concerned, while some SGRs (such as SGR 1806−20) are extremely active sources, in other cases no bursts have been detected for many years (as in the case of SGR 1627−41, that re-activated in 2008 May after a 10 year long stretch of quiescence; Esposito et al. 2008). This suggests that a relatively large number of members of this class has not been discovered yet, and may manifest themselves in the future.

On 2008 August 22, a new SGR, namely SGR 0501+4516, was discovered (the first in 10 years), thanks to the *Swift* burst alert telescope (*Swift*–BAT) detection of a series of short X-ray bursts and intermediate flares (Barthelmy et al. 2008; Holland et al. 2008). X-ray pulsations were observed by *RXTE* at a period of 5.7 s, confirming the magnetar nature of this source (Göğüş, Woods & Kouveliotou 2008), and its counterpart was identified in the infrared and optical bands (Fatkhullin et al. 2008; Rea et al. 2008b; Rol et al. 2008; Tanvir & Varricat 2008). Prompt radio observations to search for the onset of radio pulsation and of a persistent counterpart failed to reveal any emission in this band in the first days after the outburst activation (Gelfand et al. 2008; Hessels et al. 2008; Kulkarni & Frail 2008).

In this paper, we present a series of five *XMM–Newton* observations of SGR 0501+4516; the first one was performed only 1 day after the SGR activation and the last one after 38 days. We also report on two *INTEGRAL* observations; the first was performed almost simultaneously with the second *XMM–Newton* observation, while the other one was performed soon after the fourth *XMM–Newton* pointing. We used the *Swift* X-ray telescope (*Swift*–XRT) monitoring to model the outburst decay and the spin period evolution of the source until $\sim$160 days after the onset of the bursting activity. We also report on the 1992 *ROSAT* observation of its quiescent counterpart. We present details of the observation and analysis in Section 2 and results in Sections 3 and 4. Discussion follows in Section 5.

2 OBSERVATIONS AND ANALYSIS

2.1 *XMM–Newton*

The *XMM–Newton* Observatory (Jansen et al. 2001) observed SGR 0501+4516 on 2008 August/September (see Table 1) with the European Photon Imaging Camera (EPIC) instruments (pn and MOSs; Strüder et al. 2001; Turner et al. 2001), the reflecting grating spectrometer (RGS; den Herder et al. 2001) and the optical monitor (OM; Mason et al. 2001).

Data were processed using SAS version 7.1.0 with the most up to date calibration files (CCF) available at the time the reduction was performed (2008 October). Standard data screening criteria were applied in the extraction of scientific products. Soft proton flares were not observed in any of the observations, resulting in the total on-source exposure times listed in Table 1.

2.1.1 EPIC and RGS

For four of the observations, the pn camera was set in SMALL WINDOW mode in order to reduce pileup, while for the 2008 September 30 observation it was in LARGE WINDOW mode. The MOS1 camera was in FULL FRAME for the first observation and in SMALL WINDOW for all

Table 1. Top: summary of the first five *XMM–Newton* observations of SGR 0501+4516. The exposure time refers to the pn camera. Count rates are background corrected, and refer to the pn in SMALL WINDOW, except for the last observation which was in LARGE WINDOW. Bottom: timing properties of SGR 0501+4516. The pulsed fraction is defined as the background corrected (max-min)/(max+min) in the 0.3–12keV energy band. The number of bursts refers to spikes detected at >35 count s^{-1}.

Parameters	2008-08-23	2008-08-29	2008-08-31	2008-09-02	2008-09-30
Start (UT)	01:07:36	07:10:28	12:09:45	10:00:38	02:18:44
End (UT)	14:35:33	13:58:20	14:59:58	15:41:49	11:22:15
Exposure (ks)	48.9	24.9	10.2	20.5	31.0
Counts s^{-1} (pn)	8.520 ± 0.016	7.08 ± 0.02	6.60 ± 0.03	6.05 ± 0.02	3.23 ± 0.01
Pulse Period (s)	5.7620694(1)	5.7620730(1)	5.7620742(1)	5.7620754(1)	5.7620917(1)
Pulsed fraction (per cent)	41(1)	35(1)	38(1)	38(1)	43(1)
Number of bursts	80	2	0	0	0

the other pointings. On the other hand, the MOS2 was in TIMING mode, except for the last observation where it was set in SMALL WINDOW mode. All other MOS CCDs were in PRIME FULL WINDOW mode. Thick filters were used for all the instruments, and pileup was present only in the first MOS1 observation, which we ignored in the rest of the analysis. No transients were present in any imaging camera, so we are confident that the MOS2 in non-imaging mode did not collect photons from anything else than our target.

We performed a two- or one-dimensional point spread function (PSF) fitting, for the data obtained with the EPIC cameras in imaging mode or timing mode, respectively. The extraction radius was chosen in such a way as to obtain more than 90 per cent of the source counts.

We then extracted the source photons, for the cameras setup in imaging mode, from a circular region with 30 arcsec radius, centred at the source position [RA 05:01:06.607, Dec. +45:16:33.47 at J2000, with a 1σ error of 1.5 arcsec which refers to the absolute astrometric *XMM–Newton* accuracy (Kirsch et al. 2004)].[1] The background was obtained from a similar region as far away as possible from the source location in the same CCD. For the MOS2 camera in timing mode, we extracted the photons from RAWX 274−334, and a similar region was used for the background extraction, although as far as possible from the source position. Only photons with PATTERN ≤ 4 were used for the pn, with PATTERN ≤ 12 for the MOS2 when in imaging mode and with PATTERN $= 0$ were used for MOS2 observations in timing mode. All the photon arrival times have been corrected to refer to the barycentre of the Solar system.

Thanks to the high timing and spectral resolution[2] of the pn and MOS cameras, and to the high spectroscopic accuracy of the RGS, we were able to perform timing and spectral analysis, as well as pulse-phase spectroscopy. Both the MOSs and pn cameras gave consistent timing and spectral results, and we report only on the pn results (see Table 1 for the pn source count rates for all five observations), and the RGS is used only to constrain the presence of narrow lines (see Section 4).

For the timing (Section 3) and spectral analysis (Section 4), we removed the bursts observed in the first two observations (August 23 and 29; also see Fig. 1) discarding all the photons corresponding to intervals where the source count rate exceeded 35 counts s^{-1} (a detailed analysis of the bursts themselves will be reported elsewhere).

[1] Consistent with the more accurate *Chandra* determination: RA 05:01:06.756, Dec. +45:16:33.92 (0.11 arcsec error circle; Woods, Gogus & Kouveliotou 2008)

[2] See http://xmm.esac.esa.int/ for details.

2.1.2 *Optical monitor*

25 OM images of the field were obtained simultaneously to the X-ray observations through the $UVW1$ lenticular filter. One further image was obtained through the U filter. The $UVW1$ has an effective transmission range of $\lambda = 2410$–3565 A, peak efficiency at λ2675 A, full-width half-maximum image resolution of 2 arcsec and a Vega-spectrum zero point of $m = 17.20$. The U has an effective transmission range of $\lambda = 3030$–3890 A, peak efficiency at $\lambda = 3275$ A, full width at half-maximum image resolution of 1.55 arcsec and a Vega-spectrum zero point of $m = 18.26$. Modulo-8 fixed photon pattern and scattered background light were removed from individual images before correcting optical distortion and converting images to J2000 celestial coordinates. The *XMM–Newton* star trackers provide absolute pointing accurate to 1.8 arcsec. To refine astrometry, a correction is performed to individual images by cross-correlating source positions in the OM with counterparts in the USNO-B1.0 catalogue (Monet et al. 2003). The $UVW1$ images were mosaicked to produce a 70 ks summed exposure. The U-band image was accumulated over an exposure time of 4 ks. Aperture photometry was performed on the source position of SGR 0501+4516 using a standard 17.5 arcsec radius circular aperture for the $UVW1$ image and 3 arcsec for the U image, consistent with the calibrated zero point.

No *XMM*–OM source is detected within this aperture to 3σ magnitude upper limits of $m_U > 22.1$ and $m_{UVW1} > 23.7$ (see Fig. 2). We also searched for possible counterparts to the X-ray bursts in the XMM-OM exposures in the $UVW1$ filter during the first *XMM–Newton* observation. We did not find any signature for such bursts in the $UVW1$ filter with a 3σ upper limit on each 4 ks image of $m_{UVW1} > 22.05$.

2.2 *Integral*

INTEGRAL (Winkler et al. 2003) observed SGR 0501+4516 twice, soon after its discovery: the first observation (orbit 717), soon after its discovery, started on 2008 August 27 at 00:31 (UT) as a Target of Opportunity (ToO) observation (ended on August 28 08:36 UT), and the second observation in the framework of the Core Programme observations of the Perseus Arm region started on 2008 September 5 at 05:48 and ended at 07:40 (UT) on September 10 (orbits 720 and 721). We analysed the IBIS/ISGRI data of both observations. IBIS (Ubertini

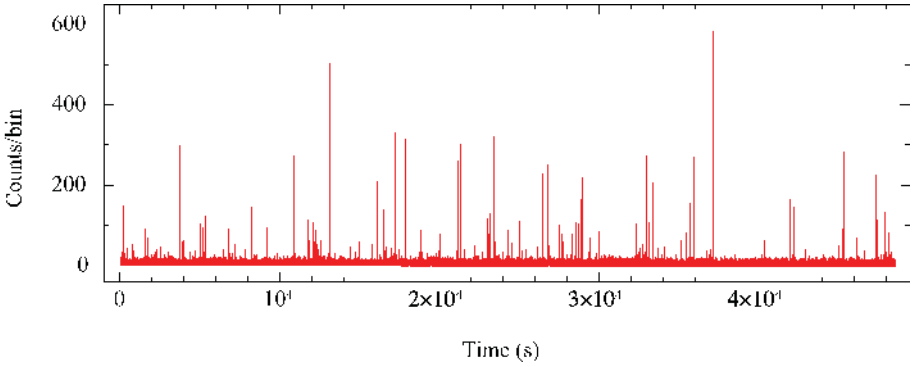

Figure 1. EPIC-pn light curve (binned at 0.5 s) of the 2008 August 23 observation. Times are in seconds from: MJD 54701 01:07:32 (UT).

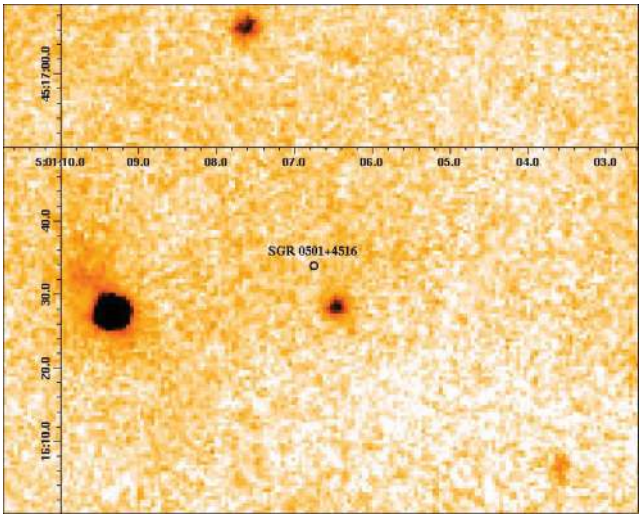

Figure 2. Co-added image of all the OM observations in the *UVW*1 filter. The four bright objects are USNO B1 stars.

et al. 2003) is a coded mask telescope with a wide (29° × 29°) field of view, sensitive in the 15 keV–10 MeV energy range. We restricted our analysis to the ISGRI (Lebrun et al. 2003) data, taken by the IBIS low-energy (15 keV–1 MeV) CdTe detector layer, since ISGRI is the most sensitive instrument on board *INTEGRAL* at energies <300 keV.

For the first observation, an effective exposure of 204 ks was accumulated at the source position. During this observation, the source was still burst active and indeed at least four weak bursts were detected in the ISGRI data (Hurley & Gotz 2008). In the 18–60 keV image, the source is detected at a $\sim 4.2\sigma$ confidence level, corresponding to a count rate of 0.31 ± 0.08 counts s^{-1}, while in the 60–100 keV band the source was detected at a $\sim 3.5\sigma$ level (0.25 ± 0.07 counts s^{-1}). Above 100 keV, the source is not detected and the 3σ upper limit is 0.2 counts s^{-1} (100–200 keV). The ISGRI response matrices were rebinned to match the above two channels and the detected flux values were used in the broad-band spectral analysis (see below Section 4).

We performed the same analysis on the Core Programme data. In this case, the exposure time was 361 ks at the position of the source. No persistent or burst emission was detected in this second observation. We could infer a 3σ upper limit in the 18–60 keV energy band of 0.18 counts s^{-1}, implying a decrease of the hard X-ray flux in about 10 days of a factor of $\sim$2.

2.3 *Swift*–XRT

The *Swift* satellite (Gehrels et al. 2004) includes a wide-field instrument, the BAT (Barthelmy et al. 2005), and two narrow-field instruments, the XRT (Burrows et al. 2005) and the ultraviolet/optical telescope (Roming et al. 2005), and discovered the bursting activity of SGR 0501+4516 thanks to the large field of view of the BAT camera (Barthelmy et al. 2008; Holland et al. 2008). We briefly report here on the *Swift*–XRT monitoring of SGR 0501+4516, and we refer to Palmer et al. (in preparation) for further details on the *Swift* observations.

Starting a few hours after the burst activation, the *Swift*–XRT camera monitored SGR 0501+4516, collecting a few tens of observations in the following 160 days. The XRT instrument was operated in photon counting (PC) mode for the first two observations, and in window timing (WT) mode for all the following observations, which ensures enough timing resolution (1.766 ms) to monitor the period changes of the source. In our analysis, we ignored the first two observations in PC mode because they were highly affected by photon pileup.

The data were processed with standard procedures using the FTOOLS task XRTPIPELINE (version 0.12.0) and events with grades 0–2 were selected for the WT data. For the timing and spectral analysis, we extracted events in a region of 40 × 40 pixels. To estimate the background, we extracted the WT events within a similar box far from the target. The event files were used to study the timing properties of the pulsar after correcting the photon arrival times to the barycentre of the Solar system. For the spectral fitting (aimed at having a reliable flux measurement over the entire outburst), the data were grouped so as to have at least 20 counts per energy bin. The ancillary response files were generated with XRTMKARF, and they account for different extraction regions, vignetting and PSF corrections. We used the latest available spectral redistribution matrix (v011) in CALDB. We removed the bursts from the XRT observations taking out all the photons corresponding to intervals where the source count rate exceeded 5 counts s^{-1}.

2.4 *ROSAT*

The *Röntgensatellit* (*ROSAT*; Snowden & Schmitt 1990; Voges et al. 1992) position sensitive proportional counter serendipitously observed the region of the sky including the position of SGR 0501+4516 between 1992 September 21 and 24, for an effective exposure time of 4.2 ks. An off-axis point source, 2RXP J050107.7+451637, was clearly detected in the observation, the position of which is consistent, within uncertainties, with that of SGR 0501+4516 as inferred by *Chandra* (Woods et al. 2008).

The *ROSAT* event list and spectrum of 2RXP J050107.7+451637 included about 260 background-subtracted photons accumulated from a circle of about 1.7 arcmin radius (corresponding to an encircled energy of ∼90 per cent). The source count rate is estimated to be $(6.6 \pm 0.5) \times 10^{-2}$ counts s^{-1} after correction for the PSF and vignetting.

3 X-RAY TIMING ANALYSIS

We started the timing analysis by performing a power spectrum of the first *XMM–Newton* observation (after having cleaned the data for the bursts; see above), and we found a strong coherent signal at ∼5.76 s, followed by eight significant harmonics. We then refined our period measurement studying the phase evolution within the observation by means of a phase-fitting technique (see DallOsso et al. 2003 for details). The resulting best-fitting period is $P = 5.762\,070(3)$ s (1σ confidence level; epoch 54701.0 MJD). The accuracy of 3 μs is enough to phase connect coherently the first two *XMM–Newton* pointings which are about 6 days apart. The procedure was repeated by adding, each time, a single *XMM–Newton* pointing. The relative phases were such that the signal phase evolution could be followed unambiguously in the five *XMM–Newton* observations, and the preliminary phase-coherent solution for these observations had a best-fitting period of $P = 5.762\,0692(2)$ s and $\dot{P} = 6.8(8) \times 10^{-12}$ s s^{-1} [MJD 54701.0 was used as reference epoch; $\chi^2 \sim 4$ for three degrees of freedom (d.o.f.)].

To better sample the pulsations in the time intervals not covered by *XMM–Newton* data, and to increase the accuracy of our timing solution, we also included the *Suzaku*–XIS observation (Enoto et al. 2009) and part of the *Swift*–XRT monitoring data set. A quadratic term in the phase evolution is required starting about 1 month after the *Swift*–BAT onset, when the pulse phases increasingly deviate from the extrapolation of the above $P - \dot{P}$ solution (see Fig. 3), resulting in an unacceptable fit ($\chi^2 \sim 110$ for 16 d.o.f.). Therefore, we added a higher order component to the above solution to account for the possible presence of a temporary or secular $\ddot{P}$ term. The resulting new phase-coherent solution had a best fit for $P = 5.7620695(1)$ s, $\dot{P} = 6.7(1) \times 10^{-12}$ s s^{-1} and $\ddot{P} = -1.6(4) \times 10^{-19}$ s s^{-2} (MJD 54701.0 was used as reference epoch; 1σ confidence level; $\chi^2 = 58$ for 45 d.o.f.), or $\nu = 0.173\,548\,754(4)$ Hz, $\dot{\nu} = -2.01(3) \times 10^{-13}$ Hz s^{-1} and $\ddot{\nu} = 5(1) \times 10^{-21}$ Hz s^{-2}. The time residuals with respect to the new timing solution are reported in Fig. 3 (central panel; empty squares). The significance of the inclusion of the cubic term is 5.3σ. Moreover, the new timing solution implies a rms variability of only 0.04 s. We note that the new timing solution is in agreement with that reported by Israel et al. (2008a).

The negative sign of $\ddot{P}$ implies that the spin-down is decreasing on a characteristic time-scale of about half a year. This might imply that a transient increase of the spin-down above the secular trend occurred in connection with the outburst onset, and that the source might now be recovering towards its secular spin-down. We note that timing components of similar strengths and with similar evolution time-scales were detected in other AXPs and SGRs following the occurrence of glitches (DallOsso et al. 2003; Dib' Kaspi & Gavriil 2008). This finding suggests that a similar event might have occurred connected to the burst and/or outburst behaviour displayed by SGR 0501+4516 in 2008 August. Correspondingly, assuming that the secular spin-down was an order of magnitude smaller than the one we measured during the outburst, our findings imply a magnetic field strength of the dipolar component in the range $7 \times 10^{13} < B_{\rm d} < 2 \times 10^{14}$ G (assuming a neutron star moment of inertia of 10^{45} g cm^2).

The 0.3–11 keV SGR 0501+4516 pulse profiles are relatively complex, with several subpeaks, though dominated by the sinusoidal fundamental component (see Fig. 4 and top panels of Fig. 9). The fundamental pulsed fraction calculated as (max − min)/(max + min) is fairly constant in time (although with some oscillations) changing from 41 ± 1 per cent during the first *XMM–Newton* pointing, to 35 ± 1 per cent (second pointing), to 38 ± 1 per cent (third and fourth pointings) and finally to 43 ± 1 per cent (last pointing; see also Table 1). At the same time, both the shape and the pulsed fraction change as a function of energy within each pointing (see Figs 5 and 6).

The *ROSAT* photon arrival times were corrected to the barycentre of the Solar system and a search for coherent periodicities was performed in a narrow range of trial periods (6.1–5.5 s; we assumed a conservative value of $|\dot{P}| = 6 \times 10^{-10}$ s s^{-1}) centred around the 2008 August period. No significant peaks were found above the 3σ detection threshold. The corresponding upper limit to the pulsed fraction is about 50 per cent.

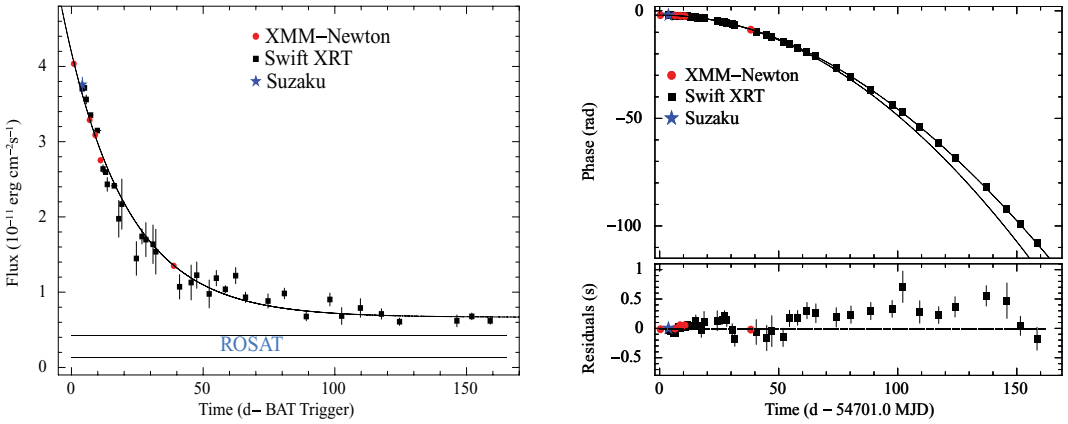

Figure 3. Left-hand panel: the outburst decay of the persistent X-ray flux of SGR 0501+4516 fitted with an exponential function (see Section 5 for details). We refer here as BAT trigger: MJD 54700.0 12:41:59.000 (UT). The fluxes are absorbed and in the 1–10 keV energy range for *XMM–Newton*, *Swift* and *Suzaku*, while the *ROSAT* flux is extrapolated to the same band and refers to two different spectral models (see Section 4 for details).Right-hand panel: the 0.5–10 keV pulse phase evolution with time, together with the time residuals with respect to the phase coherent timing solution discussed in the text and including $P/\dot{P}/\ddot{P}$ components. The solid lines in the upper panel represent the timing solution with (top line) and without (low line) the cubic term.

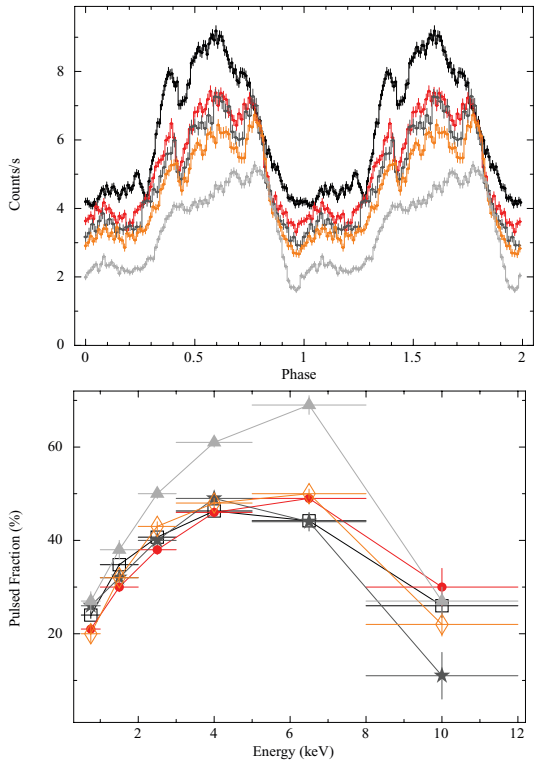

Figure 4. Top panel: pulse profiles of the five *XMM–Newton* observations in the 0.3–12 keV energy band. Bottom panel: pulsed fraction dependence with energy for the same observations. In both panels, the black, red, dark grey, orange and light grey colours refer to the five observations ordered by increasing epoch.

4 SPECTRAL ANALYSIS

For the spectral analysis, we used source and background photons extracted as described in Section 2. The response matrices were built using ad hoc bad-pixel files built for each observation. We use the XSPEC package (version 11.3, and as a further check also the 12.1) for all fittings, and used the PHABS absorption model with the Anders & Grevesse (1989) solar abundances and Balucinska-Church & McCammon (1998) photoelectric cross-sections. We restricted our spectral modelling to the EPIC-pn camera and used only the best-calibrated energy range,[3] namely 0.5–10 keV.

4.1 Phase-averaged spectroscopy

We started the spectral analysis by fitting simultaneously the spectra of all the *XMM–Newton* observations with the standard BB plus PL model, leaving all parameters free to vary except for the $N_{\rm H}$ which was constrained to be the same in all observations. The values for the simultaneous modelling are reported in Table 2, with a final reduced $\chi^2_\nu = 1.14$ for 838 d.o.f. (see also Fig. 7). The values of the spectral parameters were not significantly different when modelling each observation separately. The measured hydrogen column density is $N_{\rm H} = 0.89 \times 10^{22}$ cm^{-2}, and the absorbed flux in the 0.5–10 keV band varied from 4.1 to 1.4 $\times$ 10^{-11} erg s^{-1} cm^{-2}, corresponding to a luminosity range of 1.2–0.42 $\times$ 10^{35} d_5^2 erg s^{-1} (where d_5 is the source distance in units of 5 kpc; see Section 5.1 for further discussion on the source distance).

In the 0.5–10 keV band, the BB component accounts for $\sim$15 per cent of the total absorbed flux throughout the outburst. The BB radius, as derived from its normalization, is smaller than the neutron star size, being compatible with a constant of $\sim$1.4 km during the first month of the outburst decay (although hints for a decrease can be seen in the last observation). If the BB emission originates from the star surface, this would imply that only a small fraction of the surface is emitting.

There is evidence that as the flux decreased the 0.5–10 keV spectrum softened during the first month after the bursting activation (see Table 2 and Fig. 7). Interestingly, the BB flux decreased much slower than the PL flux, remaining almost constant for the first 10 days, and significantly decreasing only in the last observation more than a month after the burst activation (see also Section 5, Figs 6 and 7).

Since the *INTEGRAL* observation of SGR 0501+4516 was almost simultaneous to our second *XMM–Newton* observation, we then extended our spectral modelling to the entire 0.5–100 keV spectrum of the 2008 August 29 observation. We found that the BB+PL model was no longer statistically acceptable ($\chi^2_\nu = 1.29$ for 174 d.o.f.), and that the PL used to model the soft X-ray spectrum could not account for the emission above 10 keV (as it is usually the case for SGRs; Götz et al. 2006). We then tried more complex models. In line with other magnetar spectra (Götz et al. 2006; Kuiper et al. 2006), we added a second PL to the data to account for the hard X-ray emission. The results are reported in Table 3 (see also Fig. 8), where we also report the F-test probability for the addition of a further component to the fit. We also note that an excess in the residuals at energies larger than 8 keV was present in the first *XMM–Newton* observation when fit with a BB+PL model (see Fig. 7), probably due to the presence of the same hard X-ray component detected by *INTEGRAL*, which might have been present from the beginning of the outburst. The subsequent *INTEGRAL* observation close to the fourth *XMM–Newton* observation almost a week later did not show any hard X-ray emission. Assuming (although unlikely) that the hard X-ray spectral index did not change during the flux decay, we can translate our non-detection in a 3σ flux upper limit in the 18–60 keV band of $<9.7 \times 10^{-12}$ erg s^{-1}.

To take into account the presence of this hard X-ray component, we also fit the first *XMM–Newton* observation with a BB plus two PLs, fixing the PL index of the hard PL at the value inferred from the *XMM–Newton* plus *INTEGRAL* modelling of the second observation (namely $\Gamma = 0.8$; see the first and second columns of Table 3). The addition of this component was barely significant, less than in the 2008 August 29, although in the latter case the *INTEGRAL* data were crucial in the spectral modelling. We similarly tried to model the third *XMM–Newton* observation adding this PL component but in this case the addition of this further component was not significant. As in the case of the soft X-ray component, we found that the hard X-ray flux decreased significantly during the outburst decay, being undetectable by *INTEGRAL* only 10 days after the burst activation.

Simultaneously with the second *INTEGRAL* observation, an *AGILE* observation was reported in the energy range >100 MeV, starting on August 31 and ending on September 10 (Feroci et al. 2008). During the *AGILE* observation, the source was marginally burst active. The *AGILE*–GRID gamma-ray experiment did not detected the source, with a reported 2σ upper limit of 13 $\times$ 10^{-8} photon cm^{-2} s^{-1}. Assuming an average photon energy of 500 MeV, this value corresponds to $\sim$6 $\times$ 10^{-2} keV

[3] Note that in all our fittings there is a weak spurious absorption feature at $\sim$2.2 keV, which is of instrumental nature and due to the Au edge.

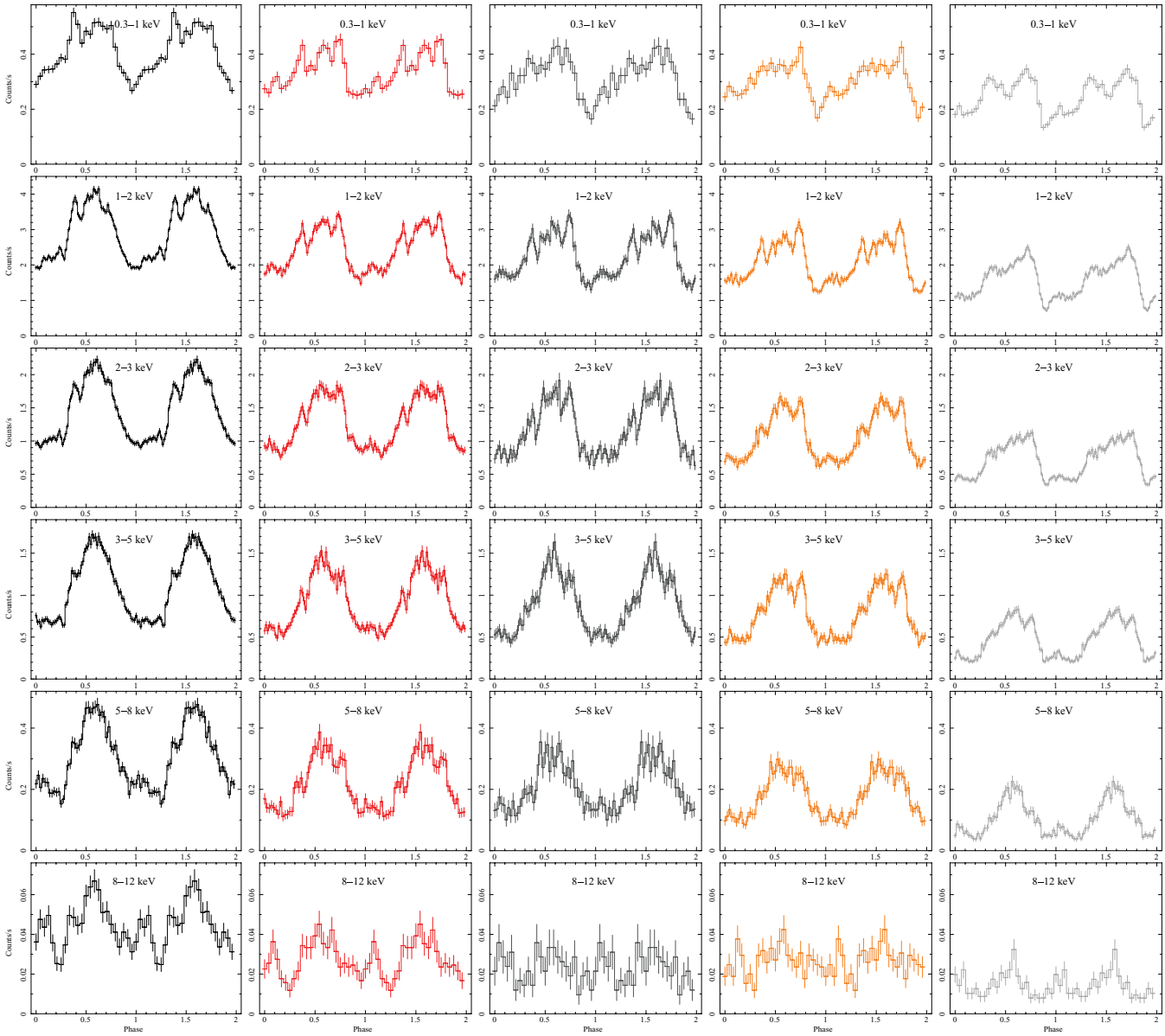

Figure 5. Pulse profiles (phase versus counts s^{-1}) as a function of energy for all five *XMM–Newton* observations of SGR 0501+4516. Each column displays one *XMM–Newton* observation with epoch increasing from left to right.

(keV cm^{-2} s^{-1} keV^{-1}), well below the extrapolation at this energy of the *INTEGRAL* PL detected during the August 29 observation (prior to the *AGILE* observation), that would predict a flux at 500 MeV of $\sim 10^3$ keV (keV cm^{-2} s^{-1} keV^{-1}). This indicates that as in the AXP cases (Kuiper et al. 2006) also in this SGR the presence of a spectral cut-off at energies between 100 keV and 100 MeV should be present spectrum during outburst.

We then studied the pre-outburst quiescent spectrum of SGR 0501+4516 as observed by *ROSAT*. The quiescent spectrum was well fitted by either a BB or PL single-component model (see Fig. 7). The best-fitting parameters are $N_{\rm H} = 6^{+5}_{-3} \times 10^{21}$ cm^{-2} and $kT = 0.38^{+0.36}_{-0.15}$ keV for the BB and $N_{\rm H} = 8^{+11}_{-4} \times 10^{21}$ cm^{-2} and $\Gamma > 0.6$ for the PL (reduced $\chi^2 = 1.08$ and $\chi^2 = 1.13$ for 17 d.o.f., respectively). The 0.1–2.4 keV observed flux is $F_{\rm X} \sim 1.4 \times 10^{-12}$ erg cm^{-2} s^{-1}, corresponding to an extrapolated 1–10 keV fluxes of 1.3 and 4.2×10^{-12} erg cm^{-2} s^{-1} for the BB and PL models, respectively. In analogy with the quiescent spectra of other magnetars, and given the slightly better reduced χ^2, we assume that the BB spectral modelling is more correct.

No spectral features were detected in the phase-averaged *XMM–Newton* spectra, with 3σ upper limits to the equivalent width of 45 and 65 eV, for a Gaussian absorption line with $\sigma_{\rm line} = 5$ eV (using the RGS spectra) and $\sigma_{\rm line} = 100$ eV (using the pn spectra), respectively.

4.2 Phase-resolved spectroscopy

We performed a phase-resolved spectroscopy (PRS) for all the *XMM–Newton* observations. We generated 10 phase-resolved spectra for each observation using the ephemeris reported in Section 3. The choice of the number of intervals was made a priori in order to have enough statistics in each phase-resolved spectrum to detect, at a 3σ confidence level, a spectral line with an equivalent width >30 eV (although none was detected). Note that given the

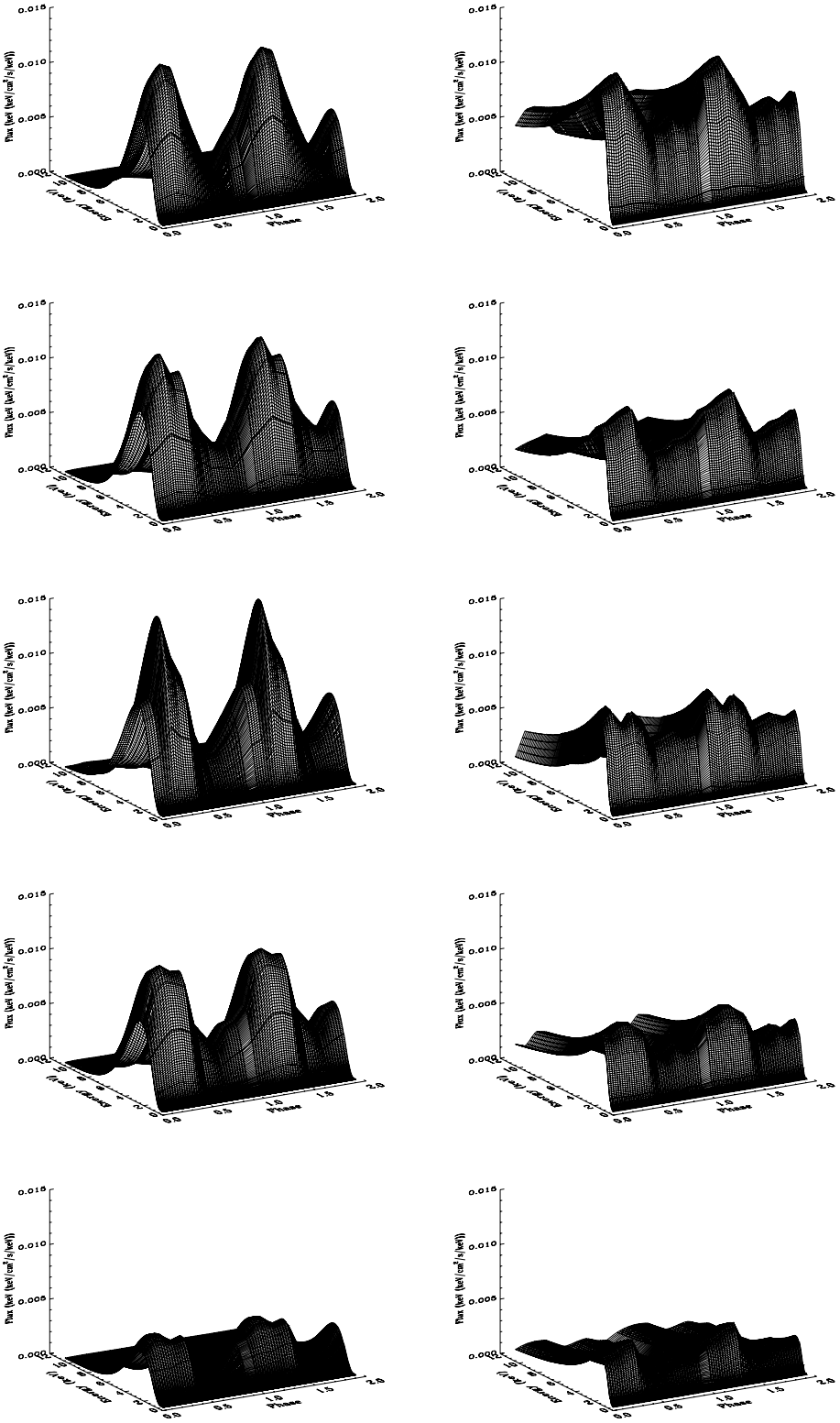

Figure 6. Three-dimensional pulse profiles for the five *XMM–Newton* observations of SGR 0501+4516 (the epoch increases from top to bottom row). Left-hand column: pulse profiles of the BB component as a function of the energy. Right-hand column: pulse profiles of the PL component as a function of the energy.

phase connection of all the five *XMM–Newton* observations (see Section 3) we can reliably follow each phase-resolved spectrum in time.

The absorbed BB plus PL model provides excellent fits for all 10 phase-resolved spectra in all the observations, both when leaving $N_{\rm H}$ free and when fixing it to the most accurate value derived in the phase-averaged fitting of all five *XMM–Newton* observations (see Table 2). In Fig. 9, we have plotted the parameters derived from the PRS analysis and compared them to the pulse profile in each observation. All the observations showed significant spectral

Table 2. Parameters for the spectral modelling of the phase-averaged spectrum of SGR 0501+4516 with an absorbed BB plus a PL [χ^2_ν (d.o.f.) = 1.14 (838)], for all five *XMM–Newton* observations.

Parameters	BB + PL				
	2008-08-23	2008-08-29	2008-08-31	2008-09-02	2008-09-30
kT (keV)	0.70 ± 0.01	0.69 ± 0.01	0.70 ± 0.01	0.69 ± 0.01	0.66 ± 0.01
BB radius (km)	1.41 ± 0.05	1.49 ± 0.05	1.42 ± 0.06	1.39 ± 0.04	1.04 ± 0.06
BB flux	2.1 ± 0.1	2.3 ± 0.1	2.15 ± 0.13	1.93 ± 0.07	0.86 ± 0.11
Γ	2.75 ± 0.02	2.92 ± 0.04	2.90 ± 0.06	2.96 ± 0.08	3.01 ± 0.04
PL flux	7.7 ± 0.1	5.8 ± 0.1	5.3 ± 0.2	4.9 ± 0.2	3.3 ± 0.1
Absorbed flux	4.1 ± 0.1	3.4 ± 0.2	3.14 ± 0.23	2.8 ± 0.1	1.4 ± 0.1
Unabsorbed flux	9.6 ± 0.1	8.1 ± 0.2	7.5 ± 0.3	7.0 ± 0.3	4.17 ± 0.11

Note. The $N_{\rm H}$ value is $(0.89 \pm 0.01) \times 10^{22}\,{\rm cm}^{-2}$ with solar abundances from Anders & Grevesse (1989). The BB radius is calculated at infinity, and assuming a distance of 5 kpc (note that in the error calculation we did not consider the uncertainty in the distance). Unless otherwise specified, all fluxes are unabsorbed, in the 0.5–10 keV range, and in units of $10^{-11}\,{\rm erg\,cm^{-2}\,s^{-1}}$. Errors are at the 90 per cent confidence level.

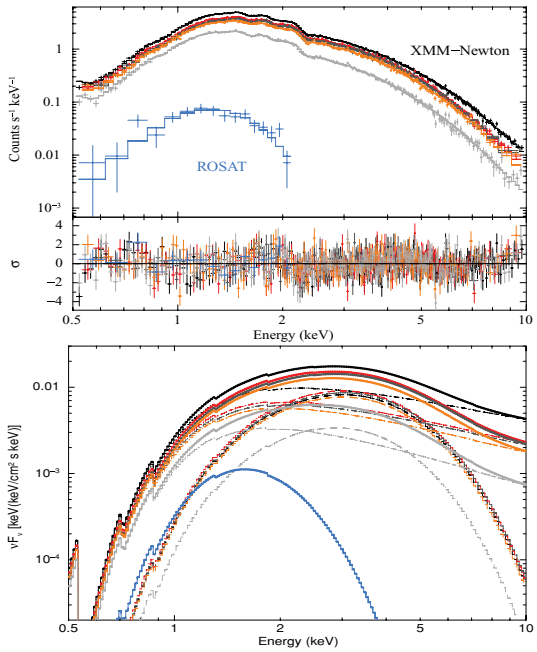

Figure 7. Phase-averaged spectra and νF_ν plot of the fitted models for the five *XMM–Newton* observations (again the black, red, dark grey, orange and light grey colours refer to the five observations ordered by increasing epoch) and the quiescent *ROSAT* counterpart (in blue).

variability with phase, as well as a general softening in time. In particular, the BB temperature and normalization follow the pulse profile shape rather well, and remaining on average rather constant throughout the outburst, with a slightly decrease in the last *XMM–Newton* observation. On the other hand, the PL parameters vary in phase and follow a more complex behaviour, with a double-peaked change of the photon index (see also Fig. 6 and Section 5 for further discussion).

5 DISCUSSION

In the last few years, thanks to the availability of wide-field X-ray instruments, as *Swift*–BAT, several outbursts from known AXP and SGR have been observed, and monitored in great detail. The detection of an outburst from SGR 0501+4516 has a special significance since this is the first new SGR discovered over a decade. In this paper, we presented a comprehensive study of the spectral and timing properties of the source in the X-rays during the entire evolution of the outburst, starting from ∼1 day after the activation and up to ∼160 days later. Our investigation is based on *XMM–Newton*, *Swift*–XRT and *INTEGRAL* data and we also re-examined *ROSAT* archival data in which the quiescent emission of SGR 0501+4516 was detected.

5.1 The outburst evolution and time-scale

Thanks to the *XMM–Newton* and *Swift*–XRT quasi-continuous monitoring (see Sections 2.1 and 2.3), we could study in detail the flux decay of SGR 0501+4516 and give an estimate of its typical time-scale. Fitting the flux evolution in the first 160 days after the onset of the bursting activity, we found that an exponential function of the form $\mathrm{flux}(t) = K_1 + K_2 \exp -(t/t_c)$ provides a good representation of the data ($\chi^2_\nu = 1.2$); the best values of the parameters are $K_1 = (0.66 \pm 0.03) \times 10^{-11}\,{\rm erg\,s^{-1}\,cm^{-2}}$, $K_2 = (3.52 \pm 0.02) \times 10^{-11}\,{\rm erg\,s^{-1}\,cm^{-2}}$ and $t_c = 23.81 \pm 0.05$ d (see Fig. 3). A fit with a PL was not found to be satisfactory ($\chi^2_\nu = 12$). Comparing the outburst decay time-scale of SGR 0501+4516 with other magnetars (see Fig. 11), there is a clear difference in time-scales. In particular, the outburst decays of other magnetars are usually fitted by two components: an initial exponential or PL component accounting for the very fast decrease in the first day or so (successfully observed only in a very few cases), followed by a much flatter PL with an index of $\delta \sim 0.2$–0.5, where $\mathrm{flux}(t) = (t - t_0)^\delta$ (see Woods et al. 2004; Israel et al. 2007; Esposito et al. 2008). A pure exponential flux decay with a time-scale of about 24 days is unusual and has been never observed before. However, we caveat that the source did not reach the quiescent level yet, hence a second component (e.g. a PL) in the flux decay can still appear at later times. Further monitoring observations will allow in the future a complete modelling of the outburst decay until the quiescent source level.

From Table 2 and Fig. 6, it is apparent that, at least in the first 10 days of the outburst, the flux of the BB component decayed more slowly than that of the PL one, both in the phase-average and the phase-resolved spectra. In particular, fitting the phase-average BB and PL fluxes of the first four *XMM–Newton* observations (see Table 2) with a linear function of the form

Table 3. Parameters of the spectral modelling of the phase-averaged spectra of the first two *XMM–Newton* observations of SGR 0501+4516 with a BB plus two PLs.

Parameters	BB + 2 PLs	
	2008-08-23	2008-08-29
$N_{\rm H}$	0.91 ± 0.02	0.93 ± 0.03
kT (keV)	0.70 ± 0.02	0.69 ± 0.04
BB_1 radius (km)	1.4 ± 0.1	1.5 ± 0.3
BB_1 flux	2.2 ± 0.1	2.7 ± 0.1
$\Gamma_{\rm soft}$	2.92 ± 0.07	3.2 ± 0.1
$PL_{\rm soft}$ flux	8.3 ± 0.1	7.1 ± 0.2
$\Gamma_{\rm hard}$	0.8 frozen	0.8 ± 0.2
$PL_{\rm hard}$ flux	3.5 ± 0.1	3.9 ± 0.2
Absorbed flux	7.9 ± 0.1	6.8 ± 0.3
Unabsorbed flux	14.3 ± 0.1	12.6 ± 0.3
χ^2_ν (d.o.f.)	1.17 (204)	1.18 (175)
F-test probability	3.1×10^{-5}	4.1×10^{-8}

Note. For the second observation, we used the quasi-simultaneous *INTEGRAL* data (see also Fig. 8 and Section 2.2). $N_{\rm H}$ is in units of 10^{22} cm^{-2}, and the BB radius is calculated at infinity, assuming a distance of 5 kpc (uncertainties on the distance have not been included). The BB and PL fluxes are calculated in the 0.5–100 keV band. Unless otherwise specified, fluxes are all unabsorbed and in units of 10^{-11} erg cm^{-2} s^{-1}. Errors are at the 90 per cent confidence level.

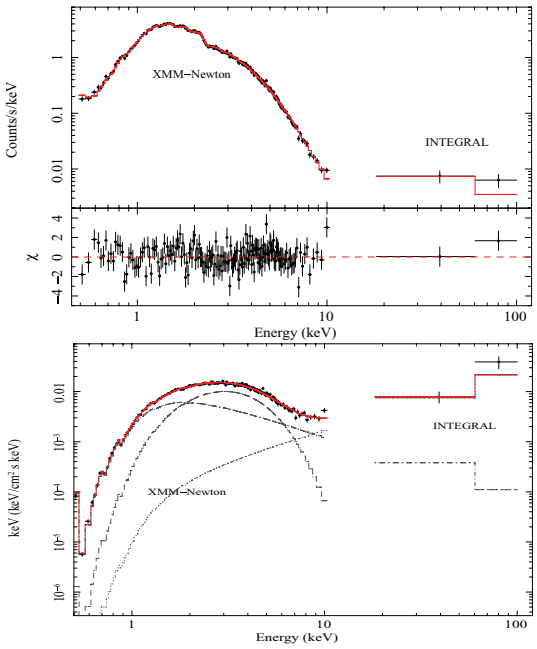

Figure 8. Phase-averaged spectra of the second *XMM–Newton* observation and the quasi-simultaneous *INTEGRAL* one, modelled with a BB plus two PLs (see also Table 3).

flux(t) = $A_1 + A_2 t$, we found a good fit for A_1(PL) = $7.9(1) \times 10^{-11}$ erg s^{-1} cm^{-2} and A_1(BB) = $2.2(1) \times 10^{-11}$ erg s^{-1} cm^{-2} and with A_2(PL) = $-0.29(1) \times 10^{-11}$ erg s^{-2} cm^{-2} and A_2(BB) = $-0.018(3) \times 10^{-11}$ erg s^{-2} cm^{-2}. While the PL flux decreased by ∼25 per cent from the first to the second observation (and kept decreasing at a reduced rate in observations three and four), the BB flux stayed approximately constant during the first four observations. Both fluxes then substantially decreased in observation five (see also Section 4.2 and next section for the evolution of the phase-resolved spectra). The relative decays of the thermal and non-thermal components observed here are reminiscent of those of CXO J167410.2−455216 after its intense burst of 2006 September 21 (Israel et al. 2007; Muno et al. 2007). Even in that case, the PL component decayed more rapidly than the BB flux (Israel et al. 2007). The faster decay of the non-thermal emission from SGR 0501+4516 is also corroborated by the non-detection of the source in the second *INTEGRAL* pointing (see Section 4).

The transient character of the hard component we detected at the beginning of SGR 0501+4516's outburst implies that, whatever the emission mechanism is, thermal bremsstrahlung in the surface layers heated by returning currents, synchrotron emission from pairs created higher up (∼100 km) in the magnetosphere (Thompson & Beloborodov 2005) or resonant up-scattering of seed photons on a population of highly relativistic electrons (Baring & Harding 2007), it has to be triggered by the source activity and quickly fade in a few days. All the previous scenarios are indeed compatible with the observed behaviour provided that a flow of highly relativistic particles is injected into the magnetosphere during the outburst. Note that this is the first time that a variable hard X-ray emission is detected for a magnetar during an outburst. Of course, our observations did not allow us to distinguish between a rapid spectral softening (as expected if the particles responsible for the emission becomes less and less energetic) and/or an overall fading of the hard component due to a decrease in its normalization (as expected if the spatial region occupied/heated by such particles shrinks or if their local density decreases).

Several investigations have suggested that the observed magnetar spectra form in the magnetosphere, where thermal photons emitted from the neutron star's surface undergo repeated resonant scatterings (Thompson, Lyutikov & Kulkarni 2002; Lyutikov & Gavriil 2006; Fernandez & Thompson 2007; Nobili, Turolla & Zane 2008a, Rea et al. 2008a). In this scenario, the spectral shape of the non-thermal component in the ∼0.1–10 keV band (and possibly also that at *INTEGRAL* energies; see Baring & Harding 2007, 2008; Nobili, Turolla & Zane 2008b) is governed by the amount of twist which is implanted in the magnetosphere as a consequence of large-scale crustal motions (starquakes). The twist must decay, due to resistive ohmic dissipation, in order to support its own currents (Beloborodov & Thompson 2007; Beloborodov 2009) and this, in turn, implies that the high-energy component of the spectrum has to fade. If either the initial twist is global or, as it seems more likely, it affects only a bundle of (closed) field lines (e.g. near a magnetic pole), the magnetosphere evolves in such a way as to confine the current-carrying ($\nabla \times \boldsymbol{B} \neq 0$) field lines closer to the magnetic axis (Beloborodov 2009). This necessarily quenches resonant upscattering because the value of the cyclotron energy in most of the region occupied by the current-carrying field lines (which now extend to large radii) drops below ≈1 keV, the typical energy of thermal photons.

Thompson et al. (2002) and Beloborodov & Thompson (2007) pointed out that the surface of a magnetar with a twisted magnetosphere is heated by the returning currents. If the twist decays, the luminosity and the area of the heated surface decrease in time. However, while the thermal component is expected to survive over the time-scale necessary to dissipate the twist energy, the non-thermal component is more short-lived, since resonant scattering is no longer possible when the current-carrying bundle becomes

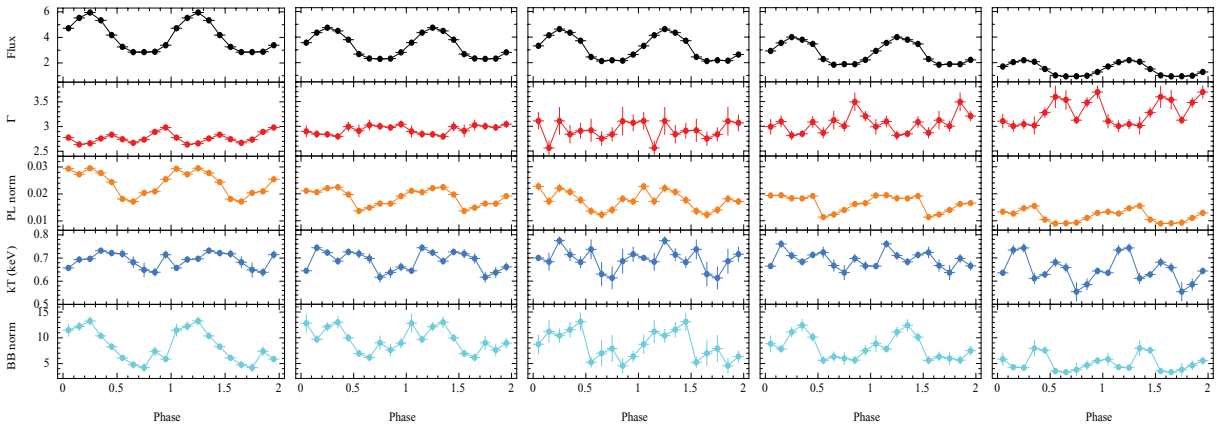

Figure 9. PRS: spectral parameters for each 0.1 phase-bin for all five observations (epoch increases from left to right). For each observation, all phase-resolved spectra were fitted simultaneously with an absorbed BB plus a PL, keeping the $N_{\rm H}$ fixed at the most accurate phase-averaged value [$N_{\rm H} = (0.89 \pm 0.01) \times 10^{22}$ cm^{-2}]. Fluxes are absorbed, in the 0.5–10 keV energy range and in units of 10^{-11} erg s^{-1} cm^{-2}. Error bars are at the 90 per cent confidence level.

too small. By comparing the theoretical expectations for a typical twist duration and luminosity, Beloborodov (2009) found an overall agreement with the observed properties of the transient AXP (TAXP) XTE J1810−197, provided that the twist was localized. In the case of SGR 0501+4516, the typical derived evolution time (∼1 month) requires both a twist confined to a small volume (angular extent $\sin^2\theta \sim 0.1$) and a modest twist angle ($\psi \sim 0.1$). The distance of SGR 0501+4516 is not known yet, but it has recently been estimated to be ∼1.5 kpc at the lowest (Aptekar et al. 2009), which implies a minimum source peak luminosity $L \gtrsim 2.5 \times 10^{34}$ erg s^{-1}. In this case, the values of the magnetospheric parameters derived above from the time-scale of the outburst evolution are too small to explain the observed luminosity in terms of dissipation of the twist energy alone ($L_{\rm twist} \sim 10^{33}$ erg s^{-1}), and the problem worsens if the source distance is larger (unless the emission has a beaming factor $\lesssim$0.1). One possibility is that part of the energy has been released impulsively in the crust because of the dissipation of the toroidal field following the starquake, as suggested to explain the decay of SGR 1900+14 and SGR 1627−41 (Kouveliotou et al. 2003; Lyubarsky et al. 2003). However, this scenario predicts a PL luminosity decline, $L \sim (t - t_0)^{\delta}$, which is not observed in SGR 0501+4516. We note that the flux decay may follow different laws in the untwisting magnetosphere model of Beloborodov (2009), and the observed different decay time-scales of the thermal and non-thermal components fit in the latter scenario.

5.2 Spectral variability with phase

To study the pulse profiles and the spectral changes in phase and time as a whole, we produced what we define hereafter as dynamic spectral profiles (DSPs), which are shown in Fig. 10. Each column in Fig. 10 is for one of the five *XMM–Newton* observations (epoch increases from left to right). Each panel shows a contour plot of the νF_ν flux as a function of phase and energy, and has been derived from the 10 phase-resolved spectra extracted as explained above. The second row refers to the total flux, as derived from the BB+PL model, while the third and the last rows show, respectively, the flux of the PL and BB components. The plots illustrate well how the source spectrum changes as phase and time, and show a clear evolution of the phase-dependent spectrum during the outburst. At energies above ∼5 keV, the PL dominates the emission at all times. From the DSPs, and by comparing the DSPs with the pulse profiles (see Fig. 10, top panel, and also Fig. 5), it is also evident that most of the subpeaks of the pulse profiles are related to the PL component (this is particularly evident in the third and fourth *XMM–Newton* observations). On the other hand, the main component of the profiles is dominated by the BB component, which is always in phase with the main peak. Moreover, by looking at Fig. 10 it is again evident how the PL component decreases in intensity on a faster time-scale than the BB component in all phases. Actually, the BB component is not only rather constant over the first four observations (covering the first 10 days after the bursting activation) but in some phases shows a rebrightening (see Fig. 6 and the third panel in the last row of Fig. 10). This is likely due to some late heating of the surface, e.g. by returning currents.

The strong phase dependence of the non-thermal component may be explained by the fact that, in the twisted magnetosphere model, both the spatial distributions of the magnetospheric currents (which act as a 'scattering medium') and the surface emission induced by the returning currents (which acts as source of seed photons for the resonant scattering) are substantially anisotropic. Even under the simple assumption where the magnetosphere is dipolar and globally twisted, the heated part of the surface and the magnetospheric charges cover two different ranges of magnetic colatitude. If the twist angle varies during the outburst evolution, both distributions would move away or towards the poles but at different rates. Of course, the situation is more complicated if the magnetospheric twist affects a limited bundle of field lines, as observations seem to indicate in SGR 1806−20 (Woods et al. 2007) and in the TAXP XTE J1810−197 (Perna & Gotthelf 2008; Bernardini et al. 2009). Recent spectral calculations have shown the resonant comptonization in locally twisted multipolar fields can give rise to a hard tail which is highly phase dependent (Pavan et al. 2009). The phase-resolved spectral evolution of SGR 0501+4516 is very complicated, but a possible explanation for the variations of the PL component in terms of a magnetic field which is locally sheared, and the shear evolves in time, seems promising.

5.3 SGR 0501+4516: AXP or SGR?

For about 20 years after their discovery, SGRs and AXPs were thought to be two distinct manifestations of highly magnetic neutron

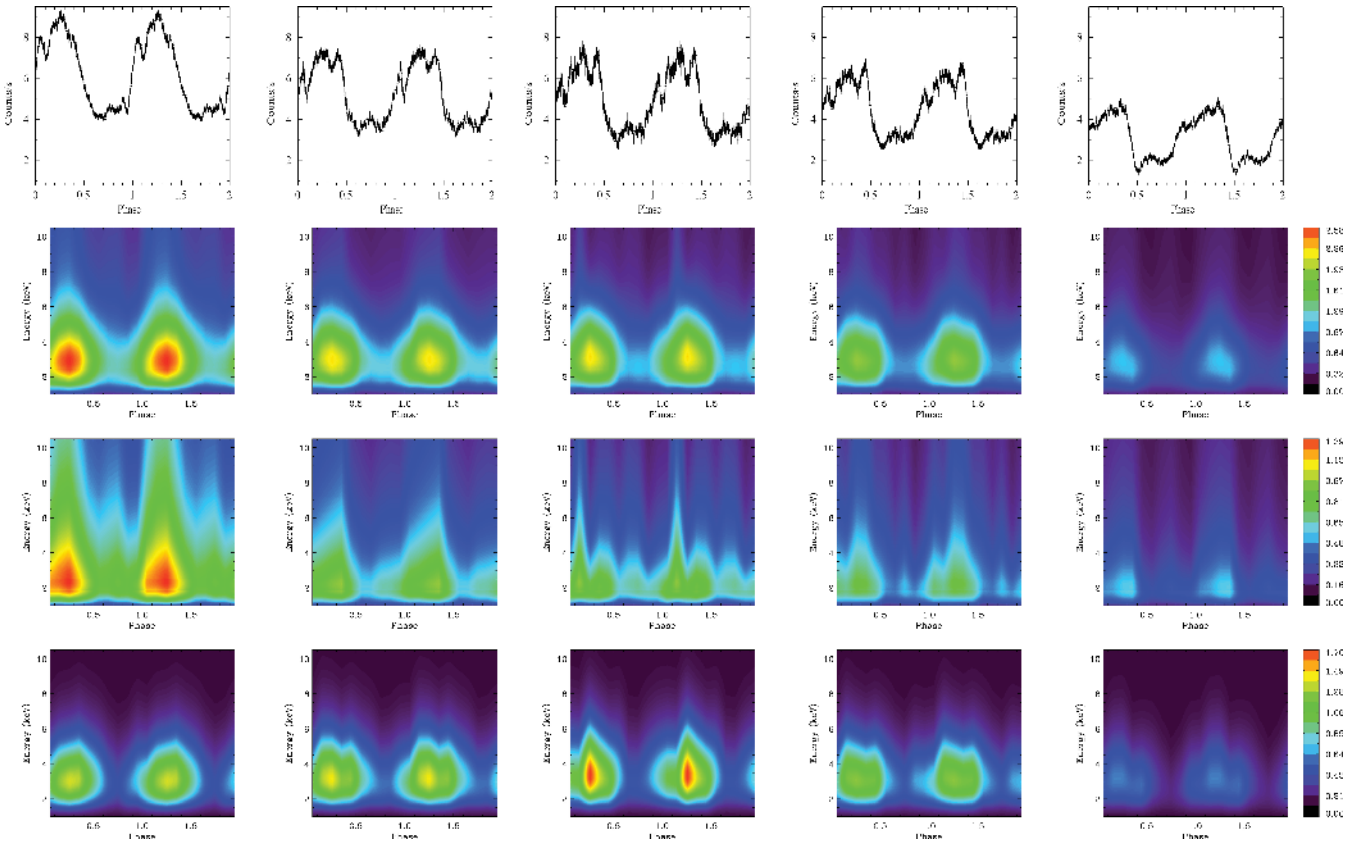

Figure 10. DSPs. Each column corresponds to one *XMM–Newton* observation (epoch increases from left to right: 2008 August 23, 29, 31, September 02 and 30). For each observation, the top panel is the 0.3-12 keV pulse profile, while the three bottom panels show in the phase/energy plane the contour plots for the total (second row), PL (third row) and BB (bottom row) νF_ν flux. The colour scale is in units of 0.01 keV (keV cm^{-2} s^{-1} keV^{-1}).

stars: the first mainly discovered and characterized by their powerful bursting activity and the second recognized as bright persistent soft X-ray emitters with spectra empirically modelled by a BB+PL and with little or no bursting activity. Furthermore, the discovery of hard X-ray emission (up to about 200 keV; Götz et al. 2006; Kuiper et al. 2006) from a few members of both classes added a further distinction, with AXPs having hard X-ray emission modelled by a second PL component (in addition to the BB+PL describing the soft X-ray emission) with $\Gamma_{\rm hard} \sim 0.8$–1, while the SGR emission was the natural extrapolation at higher energies of the PL component modelling their soft X-ray emission ($\Gamma_{\rm hard} \sim 1.5$–2.0). Over the past 6 years, the discovery of X-ray bursts from AXPs (Kaspi et al. 2003; Woods et al. 2004), and of BB components in the persistent spectrum of SGRs (Mereghetti et al. 2005,a), initiated a revision of this distinction between these two classes.

In this context, SGR 0501+4516 and 1E 1547.0−5408 can be considered the Rosetta stone for a final unification of SGRs, AXPs and the so called 'TAXPs' into a single class of 'magnetars candidates'. In fact, the properties of this new SGR, as well as the characteristics of the 2009 January 22 outburst of the AXP 1E 1547.0−5408 (Gelfand & Gaensler 2007; Halpern et al. 2008; Mereghetti et al. 2009; Israel et al., in preparation), argue for a revision of our definition of SGRs and AXPs. In particular, SGR 0501+4516's 0.5–10 keV spectrum during outburst is extremely soft ($\Gamma \sim 2.8$–3.0) compared to other SGRs ($\Gamma \sim 1.5$–2.0). Such a soft spectrum has been observed in the persistent emission of SGRs only during the 'quiescent' (burst-quiet) phases of SGR 1627−41 and SGR 0526−66 (Kouveliotou et al. 2003; Kulkarni et al. 2003; Mereghetti et al. 2006b). Furthermore, the spectrum of the quiescent X-ray counterpart of SGR 0501+4516 (see Sections 2.4 and 4) is far too soft for an SGR, while resembles the pre-outburst spectrum of the TAXP XTE J1810−197 (Gotthelf et al. 2004).

The name SGR 0501+4516 came from the strong bursting activity (see e.g. Aptekar et al. 2009; Enoto et al. 2009) which led to its discovery. However, bursts as bright and numerous as those observed from this source and other SGRs have recently been observed from the AXP 1E 1547.0−5408 in 2009 January (Gronwall et al. 2009; Savchenko et al. 2009; von Kienlin & Connaughton 2009), which emitted bursts as powerful as a typical SGR intermediate flares (Mereghetti et al. 2009).

Another piece of evidence for the AXP-like behaviour of SGR 0501+4516 and the SGR-like behaviour of 1E 1547.0−5408 is the photon index of the variable hard X-ray component. As shown in Section 4, the photon index we measure from the *INTEGRAL* spectrum is $\Gamma \sim 0.8$, which is close to the one reported for AXPs, while the variable hard X-ray emission during the 2009 January outburst of 1E 1547.0−5408 has a photon index of $\Gamma \sim 1.4$–1.6 (den Hartog, Kuiper & Hermsen 2009), typical of SGRs.

6 SUMMARY

Thanks to the unprecedented prompt observational campaigns of *XMM–Newton*, *INTEGRAL* and *Swift*, we were able to study in

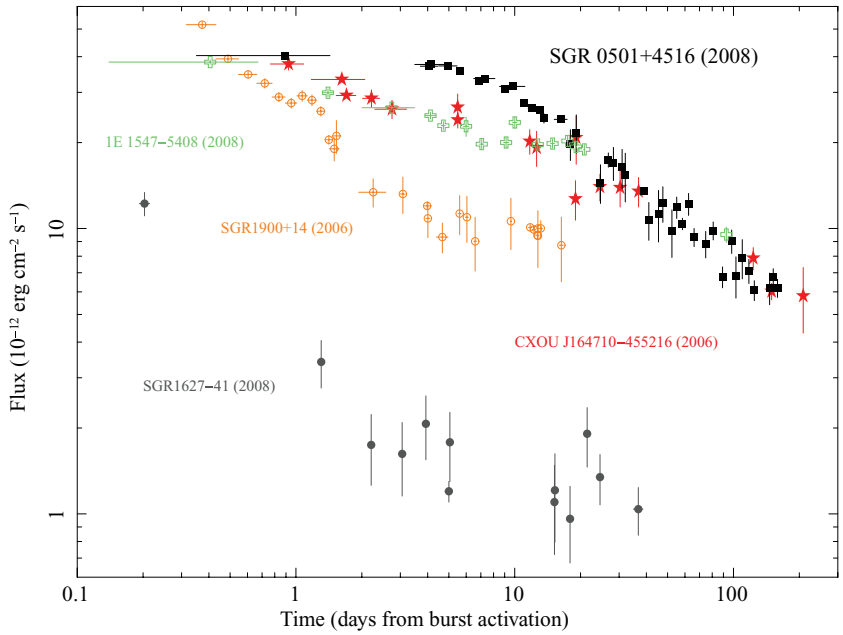

Figure 11. Flux evolution of the recent outbursts of a few magnetars (all observed with imaging instruments) compared with SGR 0501+4516. Fluxes are the observed ones in the 1–10 keV energy range, and the reported times are calculated in days from the detection of the first burst in each source. In particular, we show CXO J167410.2−455216 as red stars (Israel et al. 2007), SGR 1627−41 as grey circles (Esposito et al. 2008), SGR 1900+14 as orange empty circles (Israel et al. 2008b), 1E 1547.0−5408 as green empty crosses (Israel et al. in preparation) and SGR 0501+4516 as black squares (this work).

great detail the evolution of the first recorded outburst from the first new SGR discovered in a decade, SGR 0501+4516. Furthermore, we could compare its outburst properties with its quiescent emission as seen by *ROSAT*. We found the following.

(i) Phase-connected timing analysis of the entire X-ray outburst of SGR 0501+4516 strongly argue that this source is a magnetar candidate with a magnetic field of $B \sim 2 \times 10^{14}$ G. Furthermore, we identified a negative second period derivative of $\ddot{P} = -1.6(4) \times 10^{-19}$ s s^{-2} which implies that the spin-down rate is decreasing with time, possibly in its way to recovering to its secular pre-outburst spin-down.

(ii) A variable hard X-ray component was detected at the beginning of the outburst (see Fig. 8), and became undetectable by *INTEGRAL* sometime within 10 days after the onset of the bursting activity. This represents the first detection of a variable hard X-ray component in a magnetar over such a short time-scale.

(iii) The phase-connection of all the observations allowed us to study the evolution in time of the phase-resolved spectra. We found that on top of a phase-averaged spectral softening during the outburst decay, with the BB component decaying on a slower time-scale than the PL component (see Fig. 6), the spectral evolution also changes from phase to phase. The main peak of the pulse profile is dominated by the thermal component, while many other subpeaks are present in the profiles, which are dominated instead by the non-thermal component (see Fig. 10).

(iv) No transient optical/ultraviolet source was detected by the OM on board of *XMM–Newton* (see Section 2.1.2). Note that the optical counterpart to this source (Tanvir et al. 2008; Fatkhullin et al. 2008) is too faint to be observable by the OM, but we could constrain that no counterpart to the X-ray bursts have been observed with $m_{UVW1} > 22.05$.

(v) From a comparison with other outbursts recently detected from SGRs and AXPs (see Fig. 11), we show that contrary to other sources, in the first 160 days of its outburst, SGR 0501+4516 shows a clear exponential decay on a rather slow time-scale of about 24 days (see Fig. 3).

(vi) The discovery of SGR 0501+4516, and its AXP-like characteristics, represents another piece of evidence in the unification of the magnetar candidate class, weakening further the differences between AXPs, TAXPs and SGRs.

ACKNOWLEDGMENTS

We wish to thank Norbert Schartel for promptly approving our ToO request for the first *XMM–Newton* observation, the *XMM–Newton* team for the crucial help during the scheduling process of this monitoring program and the *INTEGRAL* mission operations team at ISOC and ESOC for their support during the ToO observations. We also thank Neil Gehrels, the *Swift* duty scientists and science planners for making the *Swift* observations possible. This paper is based on observations obtained with *XMM–Newton* and *INTEGRAL*, which are both ESA science missions with instruments and contributions directly funded by ESA Member States and the USA (through NASA), and on observations with the NASA/UK/ASI *Swift* mission. NR is supported by an NWO Veni Fellowship and thanks T. Enoto and K. Makishima for useful discussions on this source. PE thanks the Osio Sotto city council for support with a G. Petrocchi Fellowship, SZ acknowledges STFC for support through an Advanced Fellowship, KH is grateful to the U.S. *INTEGRAL* Guest Investigator programme for support under NASA Grant NNX08AC89G and PU has been supported by the Italian Space Agency through the *INTEGRAL* grant I/008/07/0.

REFERENCES

Anders E., Grevesse N., 1989, 53, 197
Aptekar R. L., Cline T. L., Frederiks D. D., Golenetskii S. V., Mazets E. P., Pal'shin V. D., 2009, ApJ, 698, L82
Balucinska-Church M., McCammon D., 1998, ApJ, 496, 1044

Baring M. G., Harding A. K., 2007, Ap&SS, 308, 109
Baring M. G., Harding A. K., 2008, in Yuan Y.-F., Li X.-D., Lai D., eds, AIP Conf. Proc. Vol. 968, Astrophysics of Compact Objects: Int. Conf. on Astrophysics of Compact Objects. Am. Inst. Phys., New York, p. 93
Barthelmy S. D. et al., 2005, Space Sci. Rev., 120, 143
Barthelmy S. D. et al., 2008, ATel, 1676
Beloborodov A. M., Thompson C., 2007, ApJ, 657, 967
Beloborodov A. M., 2009, ApJ, in press (arXiv:0812.4873)
Bernardini F. et al., 2009, A&A, 498, 195
Burrows D. N. et al., 2005, Space Sci. Rev., 120, 165
Chatterjee P., Hernquist L., Narayan R., 2000, ApJ, 534, 373
Dall'Osso S., Israel G. L., Stella L., Possenti A., Perozzi E., 2003, ApJ, 599, 485
den Hartog P. R., Kuiper L., Hermsen W., 2009, ATel, 1922
den Herder J. W. et al., 2001, ApJ, 365, L7
Dib R., Kaspi V. M., Gavriil F. P., 2008, ApJ, 673, 1044
Duncan R., Thompson C., 1992, ApJ, 392, L9
Enoto T. et al., 2009, ApJ, 693, L122
Esposito P. et al., 2008, MNRAS, 390, L34
Fatkhullin T. et al., 2008, GCN, 8160
Fernandez R., Thompson C., 2007, ApJ, 660, 615
Feroci M. et al., 2008, ATel, 1705
Gelfand J. D., Gaensler B. M., 2007, ApJ, 667, 1111
Gelfand J. D., Taylor G., Kouveliotou C., Gaensler B., van der Horst A. J., 2008, GCN, 8168
Gehrels N. et al., 2004, ApJ, 611, 1005
Göğüş E., Woods P., Kouveliotou C., 2008, ATel, 1677
Gotthelf E. V., Halpern J. P., Buxton M., Bailyn C., 2004, ApJ, 605, 368
Götz D., Mereghetti S., Tiengo A., Esposito P., 2006, A&A, 449, L31
Gronwall C., Holland S. T., Markwardt C. B., Palmer D. M., Stamatikos M., Vetere L., 2009, GCN, 8833
Halpern J. P., Gotthelf E. V., Reynolds J., Ransom S. M., Camilo F., 2008, ApJ, 676, 1178
Hessels J., Rea N., Ransom S., Stappers B., 2008, GCN, 8134
Holland S. T. et al., 2008, GCN, 8112
Hurley K., Götz D., 2008, GCN Circ., 8163
Hurley K. et al., 1999, Nat, 397, 41
Hurley K. et al., 2005, Nat, 434, 1098
Israel G. L., Campana S., Dall'Osso S., Muno M. P., Cummings J., Perna R., Stella L., 2007, ApJ, 664, 448
Israel G. L. et al., 2008a, ATel, 1837
Israel G. L. et al., 2008b, ApJ, 685, 1114
Jansen F. et al., 2001, ApJ, 365, L1
Kaspi V. M., Gavriil F. P., Woods P. M., Jensen J. B., Roberts M. S. E., Chakrabarty D., 2003, ApJ, 588, L93
Kaspi V., 2007, Ap&SS, 308, 1
Kirsch M. G. F. et al., 2004, Proc. SPIE, 5165, 85
Kouvelioutou C. et al., 2003, ApJ, 596, L79
Kuiper L., Hermsen W., Mendez M., 2004, ApJ, 613, 1173
Kuiper L., Hermsen W., den Hartog P. R., Collmar W., 2006, ApJ, 645, 556
Kulkarni S. R., Kaplan D. L., Marshall H. L., Frail D. A., Murakami T., Yonetoku D., 2003, ApJ, 585, 948
Kulkarni S. R., Frail D. A., 2008, GCN, 8130
Lebrun F. et al., 2003, A&A, 411, L141
Lyubarsky Y., Eichler D., Thompson C., 2003, ApJ, 580, L69
Lyutikov M., 2003, MNRAS, 346, 540
Lyutikov M., Gavriil F. P., 2006, MNRAS, 368, 690
Mason K. O. et al., 2001, A&A, 365, L36
Mazets E. P., Golentskii S. V., Ilinskii V. N., Aptekar R. L., Guryan Iu. A., 1979, Nat, 282, 587
Mereghetti S., Götz D., Mirabel I. F., Hurley K., 2005, A&A, 433, L9
Mereghetti S. et al., 2006a, ApJ, 450, 759
Mereghetti S. et al., 2006b, ApJ, 653, 1423
Mereghetti S., 2008, A&AR, 15, 225
Mereghetti S. et al., 2009, ApJ, 696, L74
Monet D. G. et al., 2003, AJ, 125, 984
Muno M. P., Gaensler B. M., Clark J. S., de Grijs R., Pooley D., Stevens I. R., Portegies Zwart S. F., 2007, MNRAS, 378, L44
Nobili L., Turolla R., Zane S., 2008a, MNRAS, 386, 1527
Nobili L., Turolla R., Zane S., 2008b, MNRAS, 389, 989
Ouyed R., Leahy D., Niebergal B., 2007a, A&A, 473, 357
Ouyed R., Leahy D., Niebergal B., 2007b, A&A, 475, 73
Pavan L., Turolla R., Zane S., Nobili L., 2009, MNRAS, 395, 753
Perna R., Gotthelf E. V., 2008, ApJ, 681, 522
Perna R., Hernquist L., Narayan R., 2000, ApJ, 541, 344
Rea N., Zane S., Turolla R., Lyutikov M., Götz D., 2008a, ApJ, 686, 1245
Rea N., Rol E., Curran P. A., Skillen I., Russell D. M., Israel G. L., 2008b, GCN, 8159
Rol E., Tanvir N., Rea N., Wiersema K., Skillen I., Curran P. A., 2008, GCN, 8164
Roming P. W. A. et al., 2005, Space Sci. Rev., 120, 95
Savchenko V., Beckmann V., Neronov A., Mereghetti S., von Kienlin A., Beck M., Borkowski J., Götz D., 2009, GCN, 8837
Snowden S. L., Schmitt J. H. M. M., 1990, ApJS, 171, 207
Strüder L. et al., 2001, ApJ, 365, L18
Tanvir N. R., Varricatt W., 2008, GCN, 8126
Thompson C., Beloborodov A. M., 2005, ApJ, 634, 565
Thompson C., Duncan R. C., 1993, ApJ, 408, 194
Thompson C., Duncan R. C., 1995, MNRAS, 275, 255
Thompson C., Lyutikov M., Kulkarni S. R., 2002, ApJ, 274, 332
Turner M. J. L. et al., 2001, ApJ, 365, L27
Ubertini P. et al., 2003, A&A, 411, L131
Voges W. et al., 1992, in Guyenne T., Hunt J., eds, Proc. European ISY Conf. (ISY-3), Observation and Climate Modelling through International Space Projects. ESA, Noordwijk, p. 223
von Kienlin A., Connaughton V., 2009, GCN, 8838
Winkler C. et al., 2003 A&A, 411, L1
Woods P. M. et al., 2004, ApJ, 605, 378
Woods P. M., Kouveliotou C., Finger M. H., Göğüs E., Wilson C. A., Patel S. K., Hurley K., Swank J. H., 2007, ApJ, 654, 470
Woods P., Gogus E., Kouveliotou C., 2008, ATel, 1824

This paper has been typeset from a TEX/LATEX file prepared by the author.